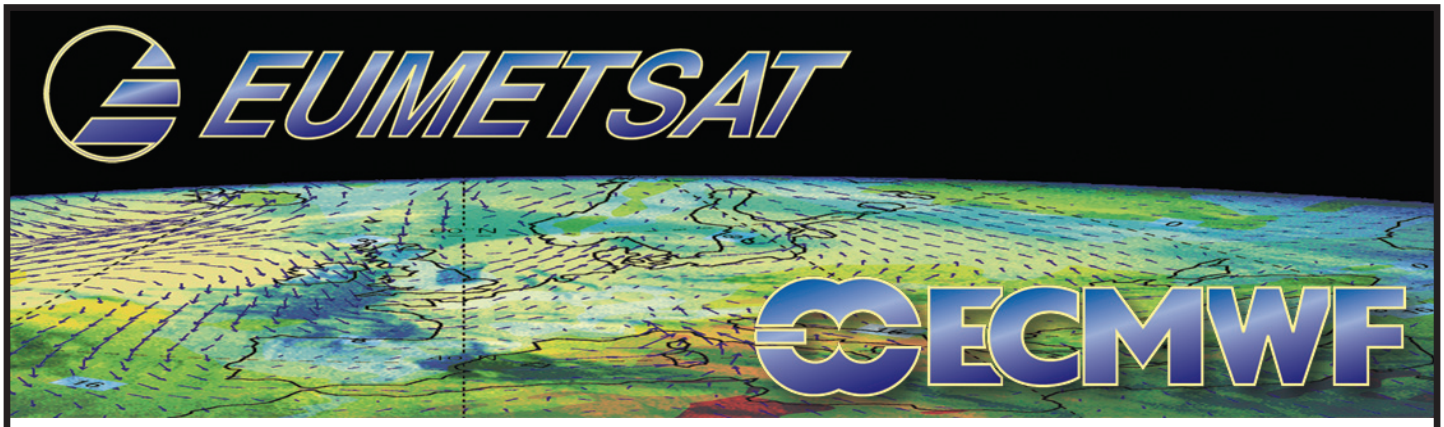

EUMETSAT/ECMWF Fellowship Programme
Research Report No. 40

The use of geostationary radiance observations at ECMWF and aerosol detection for hyper-spectral infrared sounders : 1st and 2nd years report

Julie Letertre-Danczak

February 2016

Series: EUMETSAT/ECMWF Fellowship Programme Research Reports

A full list of ECMWF Publications can be found on our web site under:
http://www.ecmwf.int/en/research/publications

Contact: library@ecmwf.int

European Centre for Medium Range Weather Forecasts
Shinfield Park, Reading, RG2 9AX, England

Contents

1 Executive Summary

This report summarizes the status and developments of my EUMETSAT Fellowship work at ECMWF. The highlights are:

Geostationary radiance observations continue to be used operationally at ECMWF and are an important element of the global observation network. No significant instrument failures or data degradations have taken place.

The operational supply of geostationary radiance data from the GOES satellites has been successfully switched from CIMSS to NESDIS.

A new facility to detect aerosols in hyper-spectral radiance observations has been developed and is now applied to METOP IASI data in ECMWF operations.

2 The monitoring and assimilation of radiances from geostationary satellites

ECMWF currently makes operational use of radiance data from five geostationary satellites, the details of which are summarized in table 1. Two EUMETSAT satellites are used at 0° and 57°E (Meteosat), one from JMA is used at 140°E (MTSAT) and two NOAA satellite are used at 135°W and 75°W (GOES).

Satellite	Position	Date Operational	Product	Channels (micron)	Status	Box Size	frequency
Meteosat-7	57°E	1^{st} May 2001	CSR	6.4 11.5	assimilated monitored	16 x 16 80 x 80 km^2	hourly
Meteosat-10	0°	24^{th} January 2013	ASR	6.2 7.3 10.8	assimilated assimilated monitored	16 x 16 50 x 50 km^2	hourly
GOES-13	75°W	28^{th} April 2010	CSR	6.5 10.7	assimilated monitored	11 x 17 50 x 50 km^2	hourly
GOES-15	135°W	25^{th} April 2012	CSR	6.5 10.7	assimilated monitored	11 x 17 50 x 50 km^2	hourly
MTSAT-2	140°E	10^{th} August 2010	CSR	6.8 10.8	assimilated monitored	32 x 32 60 x 60 km^2	hourly

Table 1: Overview of the use of CSR/ASR data in the ECMWF system in July 2015.

The figure 1 shows the coverage currently obtained from the geostationary network. For all satellites except METEOSAT-10 clear-sky radiances averaged over a defined geographical box are assimilated. For METEOSAT-10, similar spatially averaged clear sky radiances are assimilated, but additionally homogeneous cloudy radiances are used in overcast situations Lupu and McNally (2014).

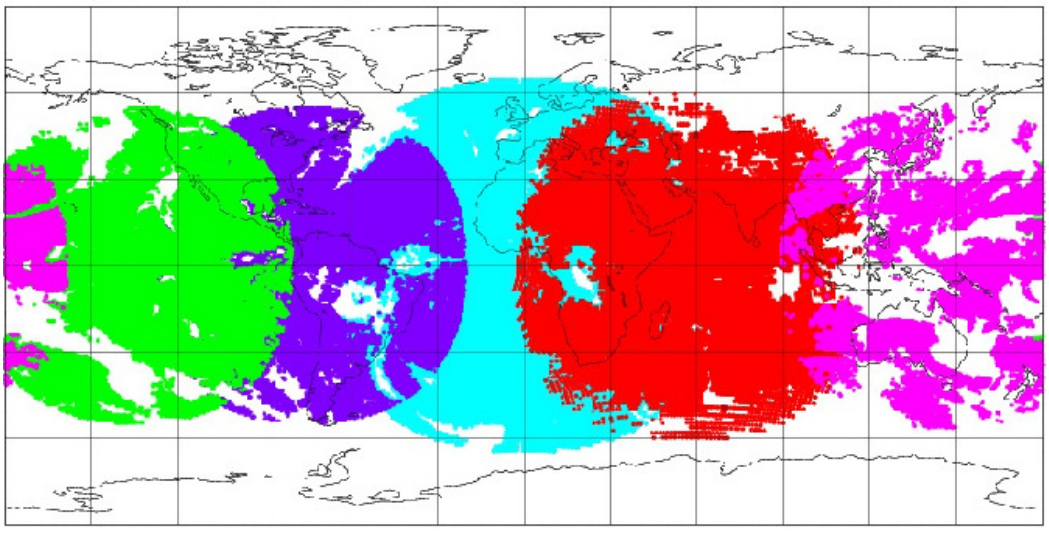

Figure 1: Global coverage for all geostationary satellites (green : Goes-15, dark blue : Goes-13, blue : Met-10, red : Met-7 and pink : MTSAT-2).

The five geostationary satellites are monitored closely by the ECMWF automatic anomaly checking system to ensure consistent data quality. There have been no serious instrument or data degradations observed during this reporting period. However, as usual intermittent blacklisting has been necessary to avoid using data during routine satellite maintainence or eclipse events. These events are detailed below.

2.1 Meteosat satellites

- **24th January 2013 :** activation of Meteosat-10.
- **13th May 2013 to 21st May 2013 :** Meteosat-7 was blacklisted during ground segment maintenance and East West Station Keeping Manoeuvre.
- **1st July 2013 to 15th July 2013 :** Meteosat-10 decontamination.
- **14th January 2014 to 27th January 2014 :** Meteosat-10 decontamination.
- **3rd December 2014 to 15th December 2014 :** Meteosat-10 decontamination.

2.2 GOES satellites

- **20th March 2013 to 26th March 2013 :** GOES West passively monitored after a Yaw Flip Manoeuvre.
- **23rd May 2013 to 12th June 2013 :** GOES East imaging stopped.
- **Since 16th April 2015 :** GOES East and West data are taken from NESDIS (CIMSS before) that implicated a slighty change on bias correction. Because the treatment applied by CIMSS and NESDIS are different, we observe changes between data from the two centres (cf figure 2 and figure 3). In general, the differences are very small, but larger discrepencies have been observed for some isolated events (e.g. 15th to 18th February 2015).

2.3 MTSAT satellite

- **24th June 2013 to 30th July 2013 :** Blacklist MTSAT-2 data due to north-south station-keeping Manoeuvre.
- **21st October 2013 to 27th January 2014 :** Blacklist MTSAT-2 data due to satellite ground system maintenance.
- **31st October 2013 to 16th December 2013 :** MTSAT-1 reactivate to replace MTSAT-2.
- **6th November 2014 to 7th January 2015 :** Blacklist MTSAT-2 data due to satellite ground system maintenance.

This year, MTSAT-2 will be replaced by Himawari-8 which was launched the 7th October 2014.

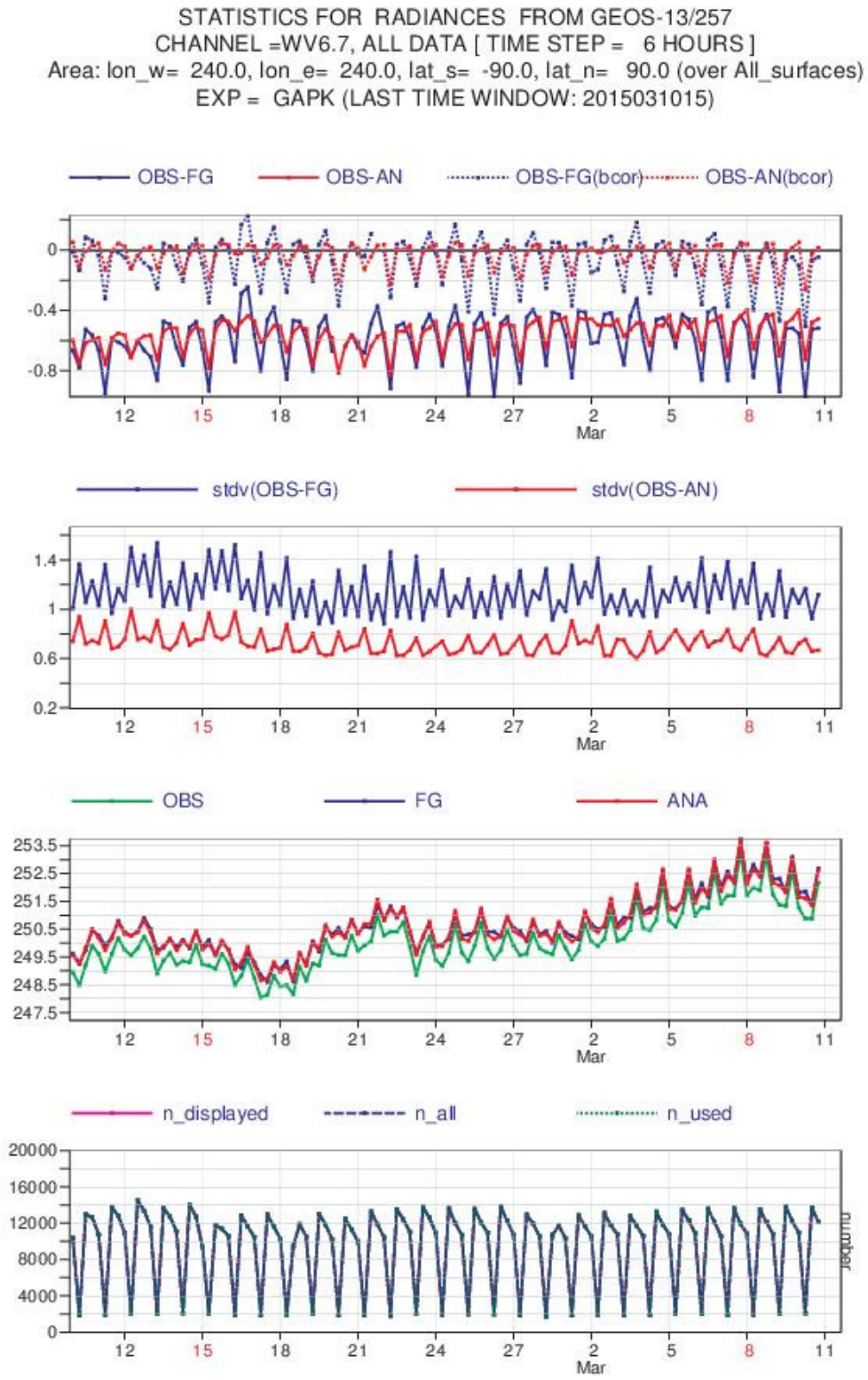

Figure 2: Time series for GOES-13 between 10th February 2015 and 10th March 2015, the data are from CIMSS.Upper panel : the difference between the observations and the first guess departure (blue), or between the observations and analyse (red) in full line, the dash line is the same data after bias correction, the second panel is the standard deviation for the same data, the third panel presents the observations (green), the first guess departure (blue) and the analyses (red), the last panel is the number of data displayed (pink), analysed (blue) and used (green).

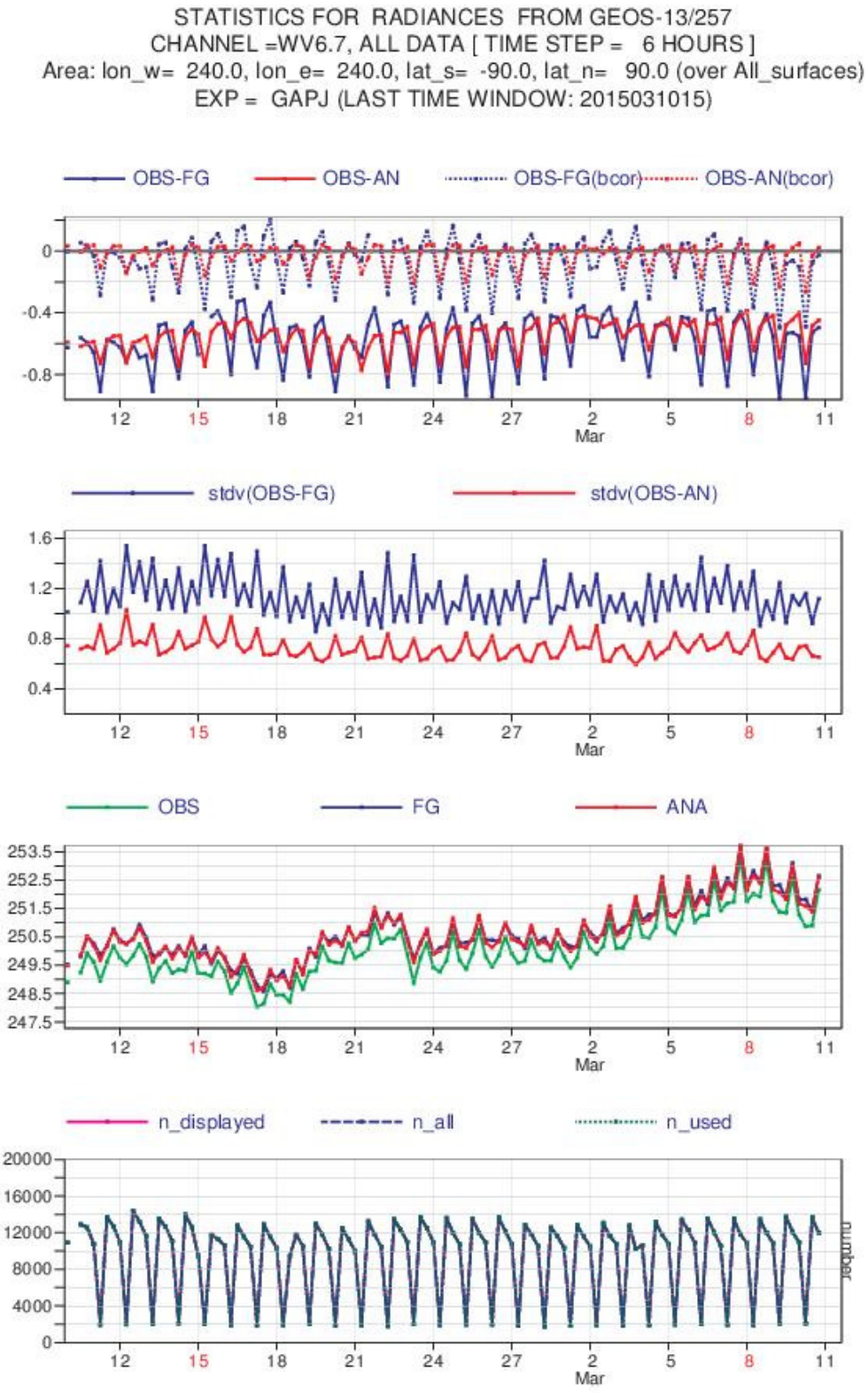

Figure 3: Time series for GOES-13 between 10th February 2015 and 10th March 2015, the data are from NESDIS. Panels are the same than the figure 2

3 Aerosol detection for hyper-spectral infrared radiances

ECMWF currently assimilates hyper-spectral radiance observations from three infrared sounders (AIRS, IASI, CRIS). The detection of clouds in these data is extremely important and employs a pattern recognition algorithm described in McNally and Watts (2003). However, the radiances observed by these infrared sounders are also affected by aerosols, and while the magnitude of the contamination is generally less than that due to clouds, the signals are significant compared to those of temperature and humidity in the data. It is thus important to detect and reject radiances displaying significant aerosol contamination.

Previous work in this area used a test brightness temperature departures in the spectral region between 1050 cm^{-1} and 1250 cm^{-1} (cf Figure 4) to provide an indication of desert dust, but was only applied to data that had already been rejected by the cloud detection scheme. It was (perhaps optimistically) assumed that the cloud detection scheme would also trap significant aerosol containation and the test was simply used to discriminate between the two causes.

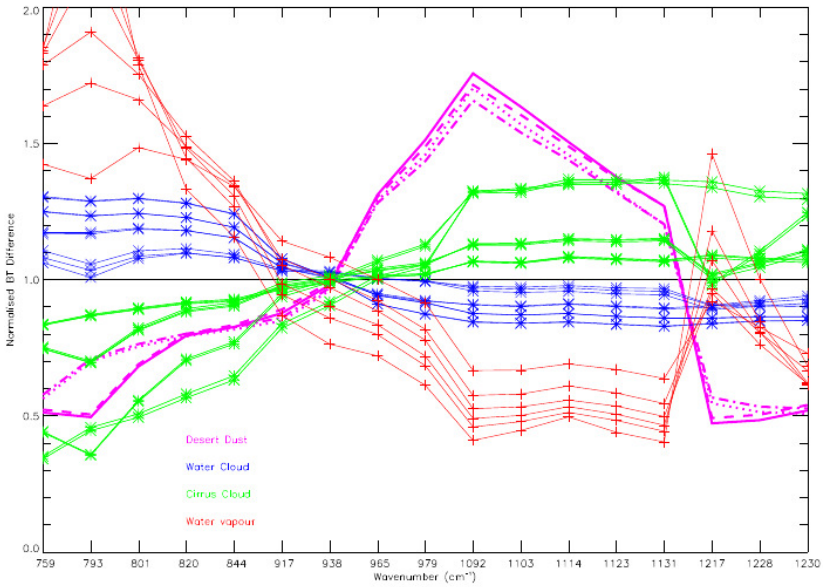

Figure 4: Impact of aerosol, cirrus clouds, water clouds and water vapour on the spectrum in the longwave window region. The frequencies shown correspond to those channels in the AIRS 324 channel subset that lie away from significant absorption line centres. Collard (2006).

A new standalone aerosol detection test has now been developed which is independent from the cloud detection and applied to all pixels. In her thesis, S. Peyridieu (Peyridieu (2010)) studied the IASI aerosol infrared spectrum (cf Figure 5) and identified some key channels which can be used to detect aerosol contamination over ocean. Specifically the new test involves thresholds applied to the following brightness temperature differences (M. Legrand and N'Doume (2001)):

$$\bar{TB}(10.207\mu m) - \bar{TB}(8.118\mu m) = BTD_1$$

$$\bar{TB}(9.172\mu m) - \bar{TB}(8.105\mu m) = BTD_2$$

As a refinement to make the test more robust against instrument noise in individual channels, ten channels are averaged around the central wavelength before the brightness temperature differences are computed. If BTD_1 and BTD_2 are less than the two empirically determined thresholds (0 and -1.7), the pixel is declared contaminated by dust. In its initial implementation this results in the full spectrum being rejected for this pixel, but in future it is hoped to refine this to only rejecting channels actually affected by the aerosol.

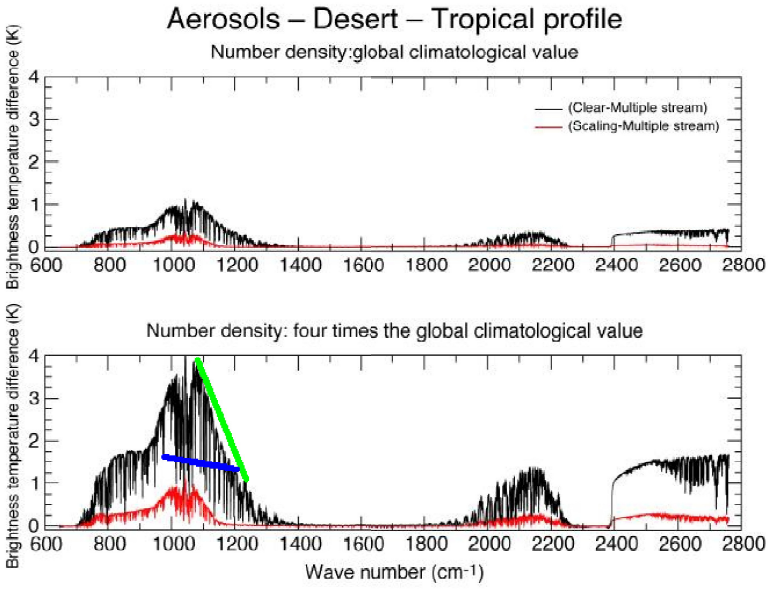

Figure 5: The radiative impact of the Continental Clean aerosol type (black curve) and the error introduced by the scaling approximation (red curve) for the tropical profile for two different aerosol number densities. Matricardi (2005)

4 Application of the new aerosol detection to IASI data

The new aerosol detection applied to IASI data from METOP-A is illustrated for three cases with a very high Aerosol Optical Depth (AOD) over the Atlantic Ocean (Figure 6), Caribean Sea (Figure 7) and Mediterranean Sea (Figure 8).

In each figure the upper panel shows where observations were previously rejected by the cloud operational detection algorithm and that the additional discrimination suggested that the cause was aerosol. The centre panel shows pixels identified as contaminated by the new aerosol test and the lower panel shows AOD at 550 nm estimated from MODIS data and the MACC (Monitoring Atmospheric Composition and Climate) data assimilation system.

On the 12th June 2013 a saharian dust plume extended over the Atlantic Ocean to the Caribean Sea between 10°N and 25°N. In the Figure 6 it can be seen that the operational system failed to detect many instances of aerosol dust over the Caribean. The extent of the aerosol dust plume is much more realistically captured with the new test by comparison to the Modis AOD retrival. A similar story is seen on the 18th June 2014 when another dust plume over Caribean Sea is examined (Figure 7). Again when we compare the extent of the detected aerosol dust plume with the MODIS and MACC estimates we see much better agreement with the new test.

On the 11th September 2013 a dust plume advected northward over Mediterranean Sea from the Sahara Desert (Figure 8). Ignoring differences over land (neither test is tuned to work over land and IASI data are not assimilated over land) we see much better agreement between the new test and the MODIS and MACC AOD estimates at 550 nm.

In summary, the cases studied so far suggest a very agreement between the new aerosol test and the MODIS and MACC estimates of AOD. Furthermore, it is apparent that there many cases of significant aerosol contamination that are not being identified and rejected by the operational system (essentially the cloud detection algorithm). When these data are assimilated, the brightness temperature signal of the aerosol will be wrongly interpreted and lead to erroneous adjustments of temperature and or humidity in the analysis. This leads us to speculate that there may some (possibly significant) benefits to implementing the new aerosol detection system in ECMWF operations. This is tested in the next section.

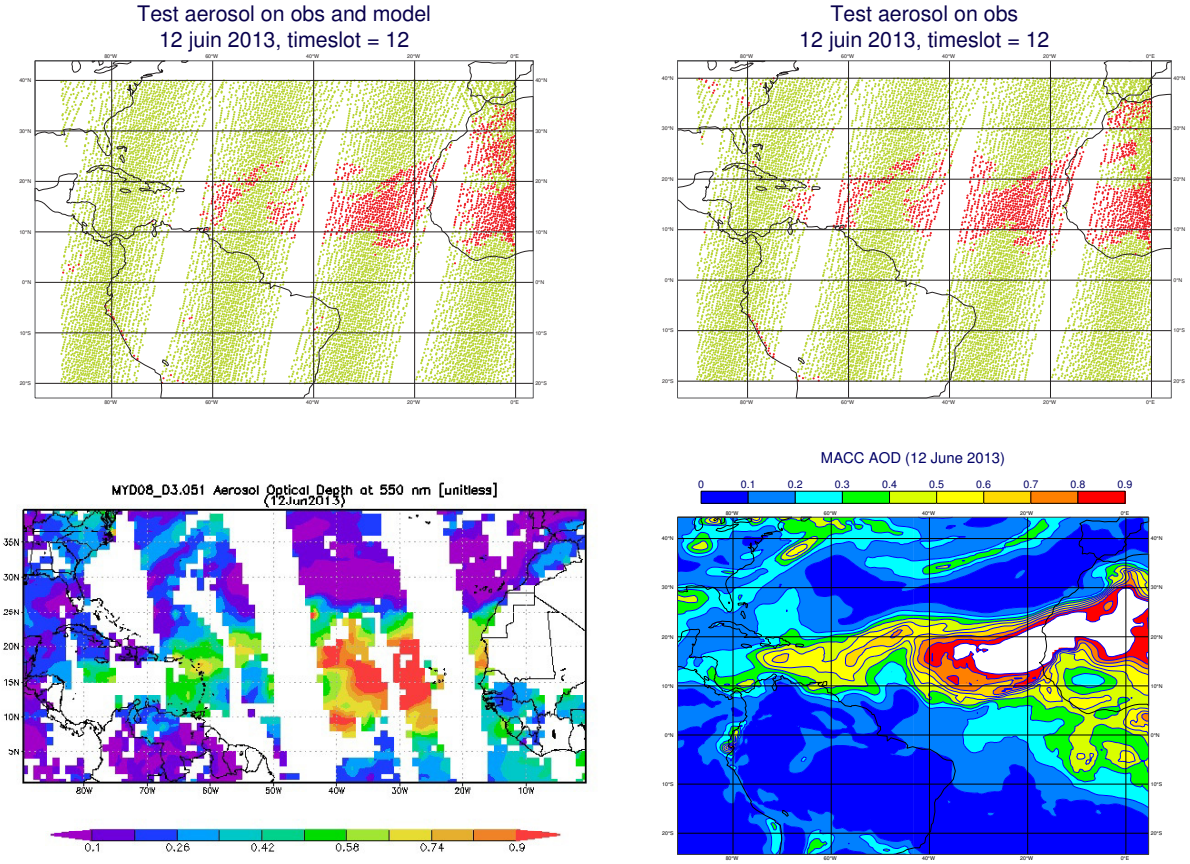

Figure 6: Aerosol detection for IASI data (upper panels, left Collard detection, right new detection), AOD at 550 nm (lower panel) from MODIS (left) and MACC (right) for the 12th June 2013 over Atlantic ocean. The pixels detected with aerosol contamination are represented in red dots, green dot means free of aerosol. if the AOD is more than 0.5, the presence of aerosol is confirmed

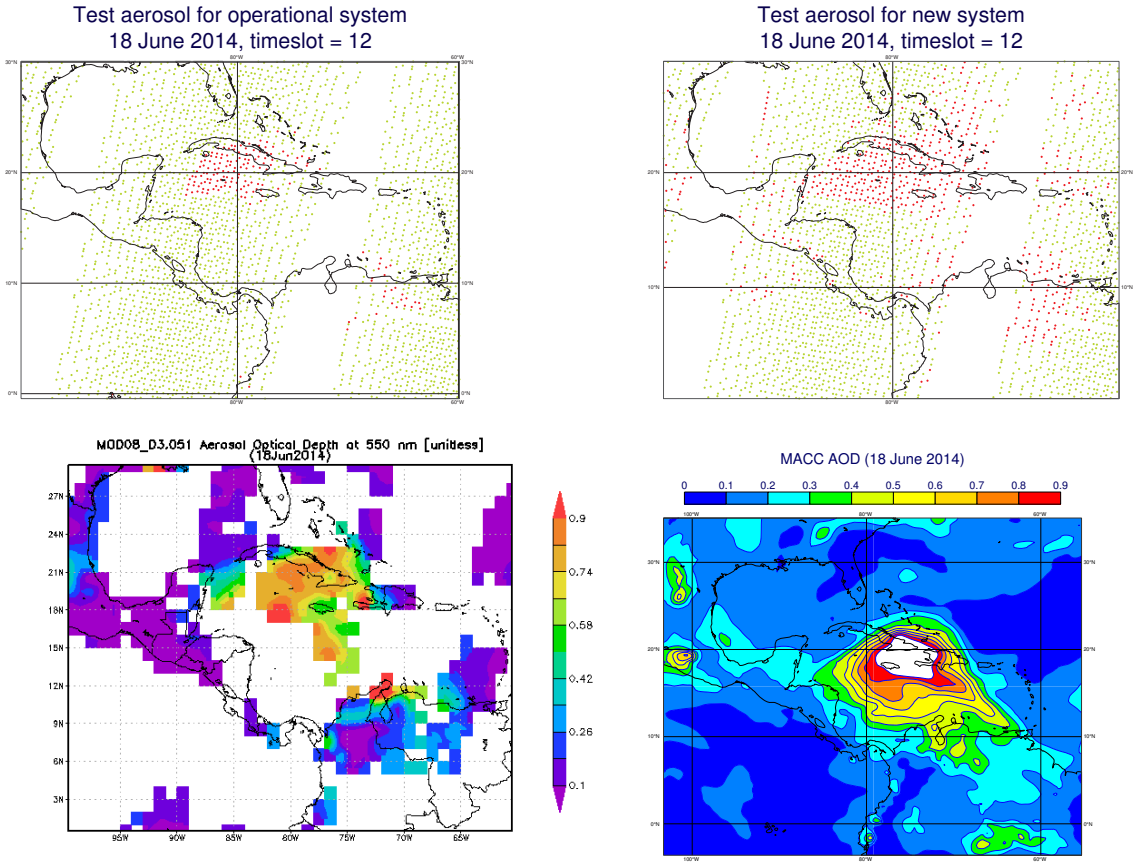

Figure 7: same as figure 6 for the 18 June 2014 over the Caribbean sea.

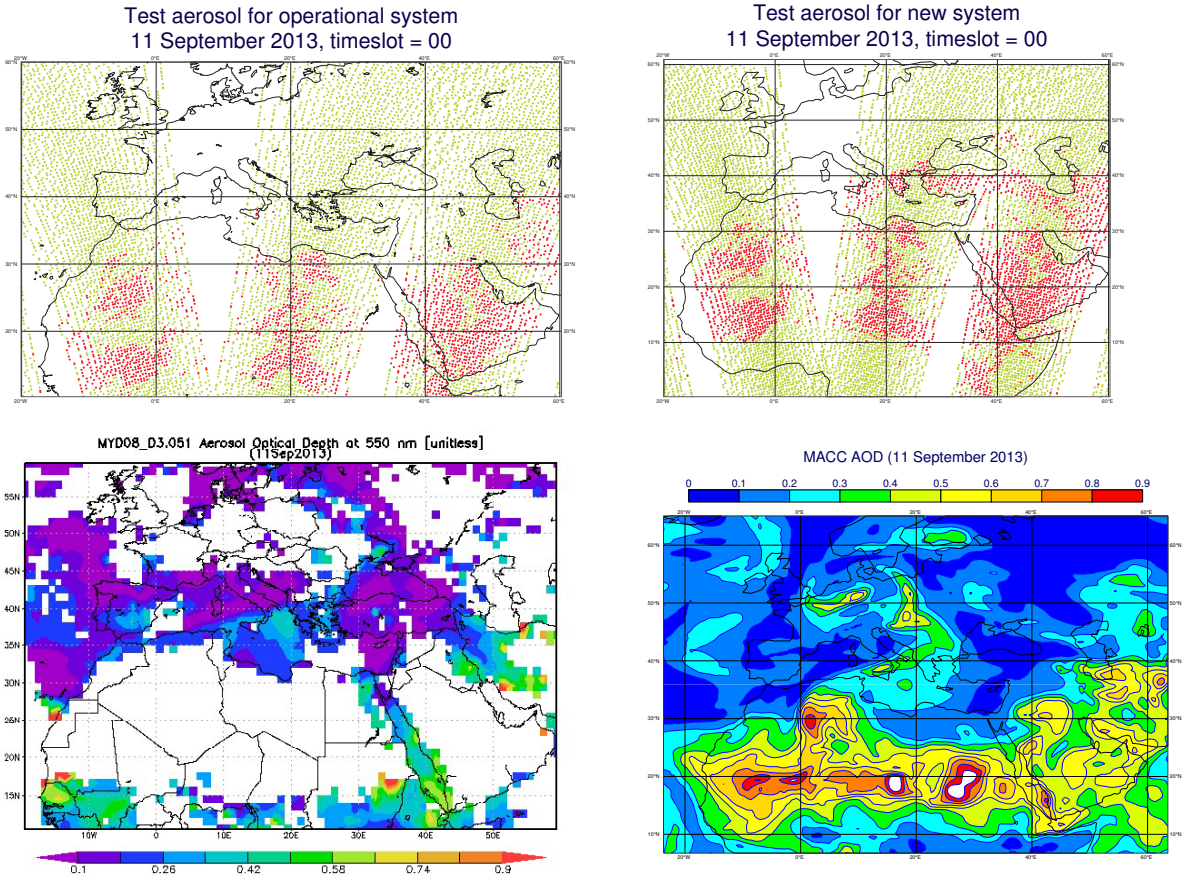

Figure 8: same as figure 6 for the 11 September 2013 over the Mediterranean sea.

5 Impact of the new aerosol detection for NWP

One month of assimilation testing has been performed (May 2014) where a control system (gal2) is compared to test system (gal1) on CY41R1. The test system rejects IASI spectra if they fail the new aerosol detection test for all pixels. For reference, an assimilation is also ran with IASI data.

In figures 6, 7 and 8 we have conclued that the new test leads to more rejections of IASI compared to the control (as expected). These additional rejections tend to be concentrated over areas known to be systematically affected by aerosol at this time of year as Caribbean sea, Mediterranean sea or Arabian Sea.

If the operational system fails to detect aerosol in a particular area it will assimilate brightness temperatures that are anomalously cold. This in turn should lead to erroneous cooling increments and in areas where this happens systematically analysis will be biased. This is confirmed when we examine the monthly mean differences of the geopotential at 500hPa for the control and test systems.

The figures 9 and 10 show the monthly mean differences of the geopotential at 500hPa for the control (new aerosol detection : g82k upper panels or operational system : g82z lower panels) and test systems (without IASI data : g82y figure 9, without infrared data : g84i figure 10).

On the figure 9, a high difference can be observed between the operational system and the new aerosol detection over the Arabian sea. In this case, the new aerosol test rejects more data in this area which if often contaminated by small dust plumes. The OSE with all infrared instruments (figure 10) shows more improvements over several area (Atlantic Ocean, Mediterannean Sea and Arabian Sea).

While these differences are small they are consistent with mean changes we see between the control and the IASI denial system. This suggests that much the mean forcing produced by the operational assimilation of IASI is due to the undetected aerosol contamination (figure 11).

The improved detection of aerosols in the analysis is further conformed when we examine the fit of the analysis to independent radiosonde observations. Figure 11, shows the departures from radiosonde temperature measurements averaged over the Tropics (most frequently affected by the presence of Dust). The standard deviation between 700hPa and 1000 hPa, where the dust layer is localized, is improvemed by around of 6%.

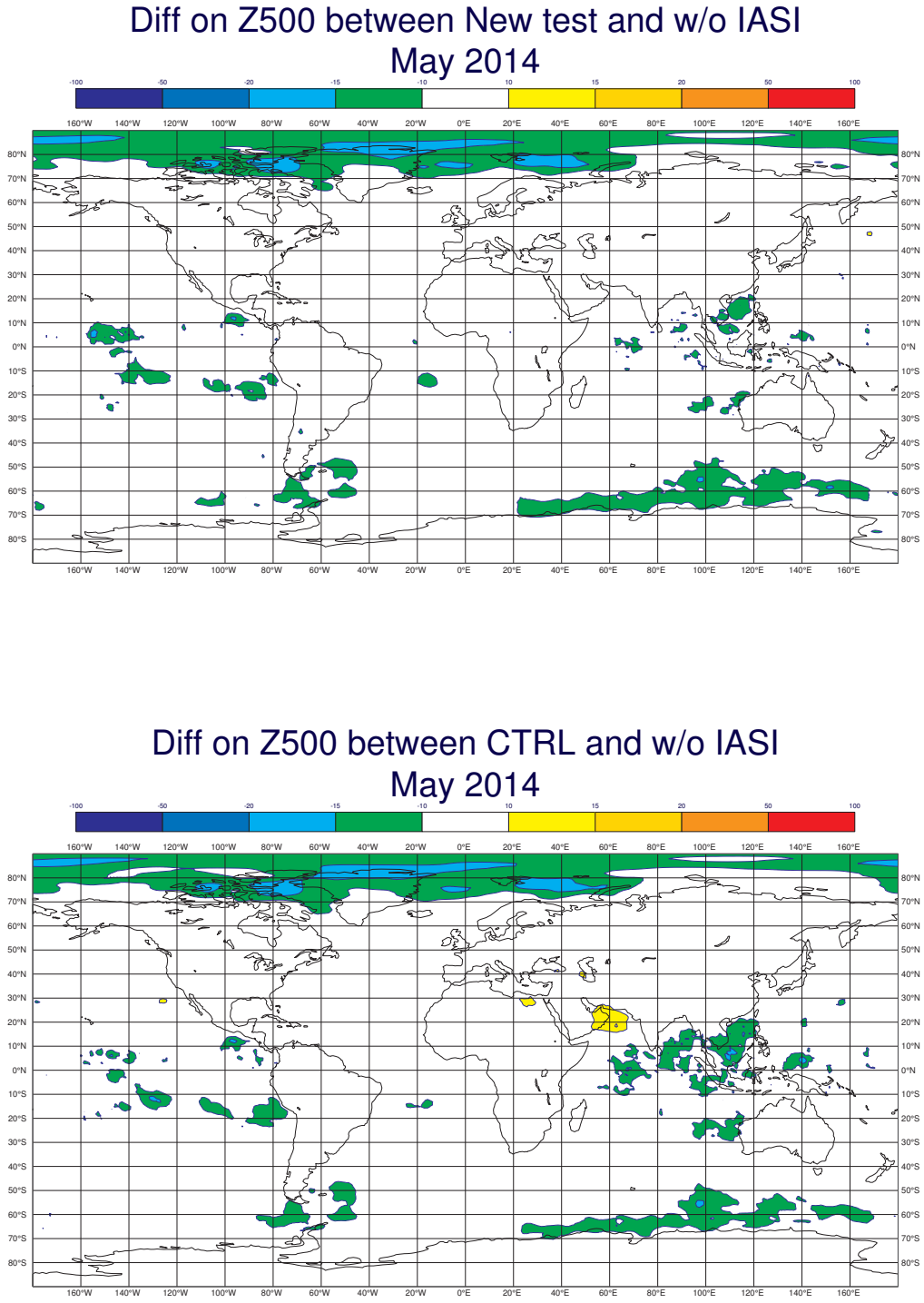

Figure 9: Difference on the geopotential at 500hPa for May 2014 between assimilation with the new test and the result of assimilation without IASI (upper) or between the result of assimilation with the operational system and the result of assimilation without IASI (lower).

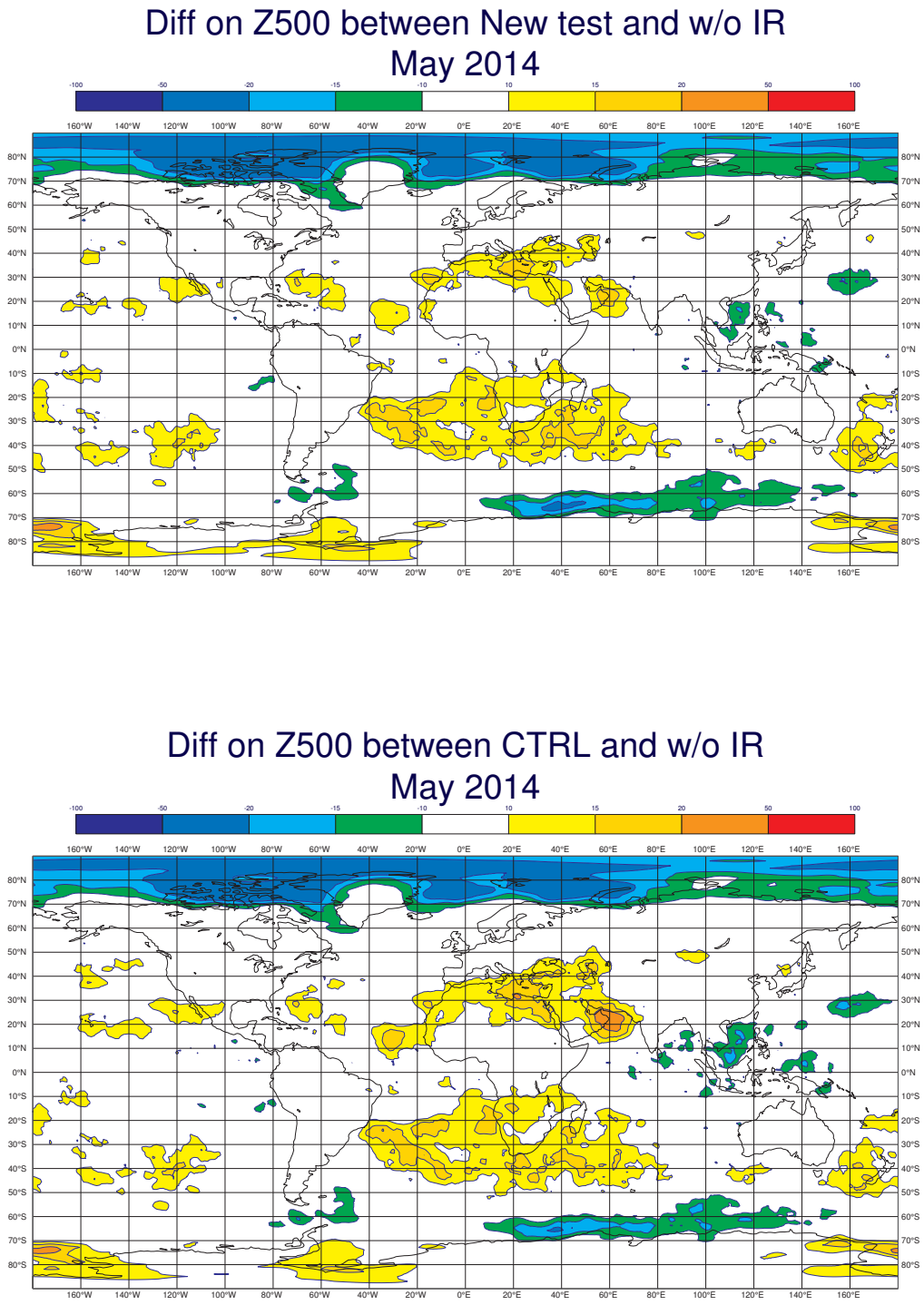

Figure 10: Difference on the geopotential at 500hPa for May 2014 between the result of assimilation with the new test and the result of assimilation without all Infrared Souders (upper) or between the result of assimilation with the operational system and the result of assimilation without all Infrared Sounders (lower).

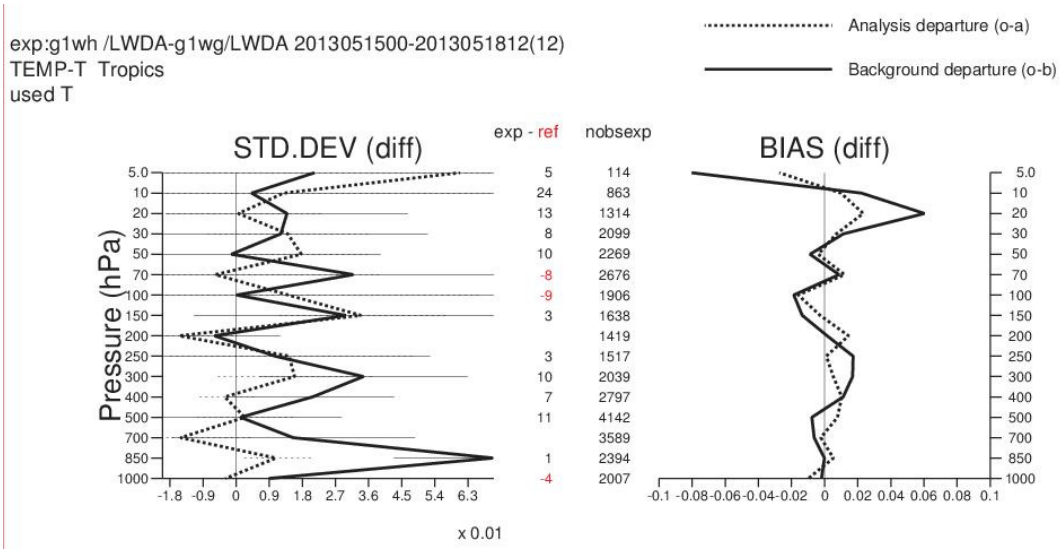

Figure 11: Difference on temperature on the Tropic area between the 15th and the 18th May 2013 between the result of assimilation with the new test and the result of assimilation with the operational system (right: standard deviation, left: bias).

6 Summary and future work

The assimilation of radiances from geostationary satellites remains in good shape and the next challenge will be to integrate data from new satellites. Preparations are already well advanced for Himawari-8 which will become operational soon and in 2016, GOES-R will be launched (operational in 2017). Meteosat Second Generation MSG-4 has been launched, but is currently parked in orbit.

Preliminary experience with the new IASI dust detection is very positive and it has been implemented in ECMWF operations (CY41R2). The extension of this test for AIRS and CrIS is almost complete and preliminary testing showing similar positive results.

Longer term new test for other important aerosol types will be developed - as well as an ability to identify the altitude of the aerosol so that only the channels actually contaminated will be rejected (not the full spectrum).

It is hoped that this work will evolve to a stage that by when MTG-IRS is launched we have a tried and tested mature facility to detect aerosol contamination. This is vitally important as MTG will observe some of the most frequently aerosol contaminated regions of the world.

7 Acknowledgements

I would like to thank Mohamed Daoui, Reima Eresmaa, Cristina Lupu, Ioannis Mallas, Marco Matricardi, Tony McNally and Kirsti Salonen for their help in this work.
Julie Letertre-Danczak is funded by the EUMETSAT fellowship programme.

References

Collard, A., 2006. Discrimination of aerosol and cloud with high-resolution infrared sounders. NWPSAF-EC-UD-004.

Lupu, C., McNally, A. P., 2014. Impact assessment of goes-15 csr and meteosat-10 asr in the ecmwf system. EUMETSAT/ECMWF Felloship Programme Research Report No.33.

M. Legrand, A. P.-F., N'Doume, C., August 2001. Satellite detection of dust using the ir imagery of meteosat, 1. infrared difference dust index. Journal of Geophysical Research No.106 (D16), 18,251–18,274.

Matricardi, M., July 2005. The inclusion of aerosols and clouds in rtiasi, the ecmwf fast radiative transfer model for the infrared atmospheric sounding interferometer. Tech. rep., ECMWF.

McNally, A. P., Watts, P. D., 2003. A cloud detection algorithm for high-spectral-resolution infrared sounders. Q.J.R. Meteorological Society No.129, 3411–3423.

Peyridieu, S., December 2010. Etablissement d'une climatologie des proprietes des aerosols de poussieres a partir d'observations hyperspectrales dans l'infrarouge. application aux instruments airs et iasi. Ph.D. thesis, Universite Pierre et Marie Curie.